lubricants

MDPI

Article

Research on the Relationship between Dynamic Characteristics and Friction Torque Fluctuation of CMGB under the Condition of Time-Varying Moment

Wenhu Zhang [1], Shili Li [1,*], Gang Zhou [2], Ningning Zhou [2], Yan Zhao [3] and Wanjia Li [4]

[1] School of Mechatronics Engineering, Henan University of Science and Technology, Luoyang 471000, China; zwh@haust.edu.cn
[2] Beijing Institute of Control Engineering, Beijing 100190, China
[3] Luoyang Bearing Research Institute Co., Ltd., Luoyang 471039, China
[4] Zhengzhou Research Institute, Harbin Institute of Technology, Zhengzhou 450000, China; wanjia@hit.edu.cn
* Correspondence: 210321010097@stu.haust.edu.cn

Abstract: In this paper, a dynamic simulation analysis model was established for CMGB (control moment gyroscope bearing) under the conditions of time-varying moment. The influences of the moment's response time, axial preload, and working temperature on the dynamic characteristics and friction torque of CMGB were analyzed, and the relevant verification tests were conducted. The results show that the friction torque fluctuation of CMGB directly corresponds to the dynamic characteristics. The faster the response time of the time-varying moment, the larger the friction torque fluctuation of CMGB. The larger preload minimizes the difference in the ball's loading state, which is the actual reason for reducing the friction torque fluctuation. Moreover, as the working temperature increases, the friction torque fluctuation of CMGB decreases.

Keywords: CMGB; time-varying moment; dynamic characteristics; friction torque; fluctuation

Citation: Zhang, W.; Li, S.; Zhou, G.; Zhou, N.; Zhao, Y.; Li, W. Research on the Relationship between Dynamic Characteristics and Friction Torque Fluctuation of CMGB under the Condition of Time-Varying Moment. *Lubricants* **2023**, *11*, 525. https://doi.org/10.3390/lubricants11120525

Received: 4 November 2023
Revised: 27 November 2023
Accepted: 1 December 2023
Published: 11 December 2023

1. Introduction

The control moment gyroscope is widely used in satellites and other spacecraft due to its high precision, high reliability, and long life [1–3]. A pair of angular contact ball bearings are the key components supporting the two ends of the rotor in the control moment gyroscope and affecting the output moment of the control moment gyroscope under high-speed conditions and the time-varying moment [4].

Researchers have conducted many studies on friction or lubrication [5,6], the dynamic characteristics of cages [7–9], structure parameters [10], and friction torque [11] for angular contact ball bearings. With the development of aerospace technology, many scholars have targeted the space ball bearing and its assemblies. Hong Wang et al. [12,13] established a nonlinear dynamic model of torque wheel bearing assembly considering the influence of bearing preload conditions, surface waviness, Hertz contact, and elastohydrodynamic lubrication. They analyzed the influence of flywheel mass eccentricity and inner/outer raceway waviness amplitude on bearing dynamic response. Wei et al. [14] introduced the structure and technical indicators of the single-frame control moment gyroscope. Qinkai Han et al. [15] used the energy theorem to establish a nonlinear time-varying dynamic model for a single-frame control torque gyro bearing assembly and analyzed the nonlinear supporting force and friction torque of angular contact ball bearings on high-speed rotors and low-speed frames. Duzhou et al. [16], aiming at the space flywheel rotor system supported by angular contact ball bearings, the lateral vibration model of established the flywheel rotor system considering the nonlinear support stiffness of angular contact ball bearings, and the effects of rotor unbalance, bearing preload, and rotor damping on the dynamic transmission of the flywheel rotor system were analyzed.

Longato Mattia M et al. [17] established the finite element model of the bearing assembly of the transient reaction flywheel. They analyzed the relationship between the surface geometric defects of the bearing parts and the micro-vibration interference generated by the reaction flywheel according to the frequency and amplitude of the bearing micro-vibration. Shankar Narayan et al. [18] studied the dynamic coupling of a rotating momentum wheel and its supporting frame to other spacecraft sub-systems. The results show that the gyroscopic moment generated by the rotating wheel body in the momentum wheel significantly influences the supporting frame. To ensure that the service life of bearing assemblies meets expectations under the steady state and variable speed conditions, Sathyan et al. [19] designed a micro oil storage lubrication system for bearing assemblies of momentum/reaction wheels. Sochting et al. [20] studied the effect of vibrations caused by responses to external excitation on space ball bearings under solid and liquid lubrication conditions. They derived the effect of vibrations at different acceleration levels on the friction torque of bearings. Hu et al. [21] investigated the temperature distribution of the bearing assembly for the control moment gyroscope under different ambient temperature conditions through experiments. Taniwaki et al. [22] investigated the dynamic characteristics of the bearing cage for the reaction wheel through experiments and numerical simulations and analyzed the relationship between bearing perturbation and cage imbalance. Based on the Newton–Euler method and momentum moment theorem, Wang et al. [23] established a dynamic model to study the effects of the mounting error of the wheel body, external micro-vibration, preload, and surface waviness on the output torque of a single-frame control moment gyroscope. Based on the rolling bearing dynamics and finite element thermal analysis, Wang et al. [24] studied the temperature distribution and its change rule of bearing assembly under different working conditions. Liao et al. [25,26] conducted experimental research on the dynamic characteristics of a space ball bearing cage and analyzed the influence of the mass center trajectory of the cage on the dynamic friction torque of the bearing. The results show that the sudden change of the friction torque is caused by the fluctuation of the trajectory of the mass center, which is independent of the shape of the trajectory. Chen et al. [27] used laser sensors to track the trajectory of the cages of ball bearings. The results show a critical rotational speed for the bearings during acceleration and deceleration, which makes the cages' trajectory transition from oscillating in a small range to circular vortexing. Zhou et al. [28] used the current of the drive motor of the friction torque testing machine to reflect the magnitude of the friction torque of the bearing assembly used for the flywheel. The results show that the bearing assembly's starting friction torque increases with the preload increase, and the assembly's friction torque during acceleration is greater than during deceleration. Xia et al. [29] established a dynamic prediction model based on grey confidence level, self-service least square method, and maximum entropy principle to dynamically predict the friction torque reliability of satellite momentum wheel bearings. Zhang [30] proposed adding micro-texture to the guide surface of the momentum wheel bearing to improve the lubrication effect between the bearing cage and the guide ring and enhance the dynamic stability of the cage. Wu et al. [31] put forward a theoretical calculation method for the optimal oil amount of flywheel bearing lubricating oil based on the theory of elastohydrodynamic lubrication and concluded that excessive and insufficient lubricating oil in flywheel bearing would lead to an increase in friction torque and the reduction of life. Based on the tribology and dynamics of rolling bearing, Cui et al. [32] investigated the effects of the preload and clearance of the cage pocket on the frictional moment of CMGB (control moment gyroscope bearing). The results show that appropriate preload and pocket clearance make the amplitude and fluctuation of the friction torque small. Deng et al. [33] studied the abnormal fluctuation mechanism of friction torque for a particular type of CMGB and found that the rub impact between the steel ball and cage, and that between the cage and the guide rib of the ring, were the main reasons for the abnormal fluctuation of the friction torque of the bearing.

In the early stage, many researchers studied the influence of rotational speed, dimensional parameters, and preload on the dynamic characteristics and friction torque of the

CMGB under steady-state conditions. However, there was little research on the response between dynamic characteristics and friction torque of the CMGB under time-variable moments, which is important for the CMGB application. This paper established a dynamic model for CMGB based on the dynamics theory of rolling bearing [34]. Consideration was given to the relative axial sliding and collision between the steel balls and the inner and outer rings, as well as between the steel balls and the cage, caused by the variable torque load in the CMGB. A comprehensive analysis of the relationship between the dynamic characteristics of the bearing and the fluctuation of the friction torque under variable torque load was conducted. And the relevant experiments for CMGB were conducted under the condition of time-varying moments.

2. Dynamic Model of CMGB

2.1. Coordinate System of CMGB

The control moment gyroscope is supported by a set of back-to-back assembled angular contact ball bearings, which support the rotation of the wheel body and use a porous oil-containing polyamide cage. A coordinate system was established to build the dynamic bearing model, as shown in Figure 1.

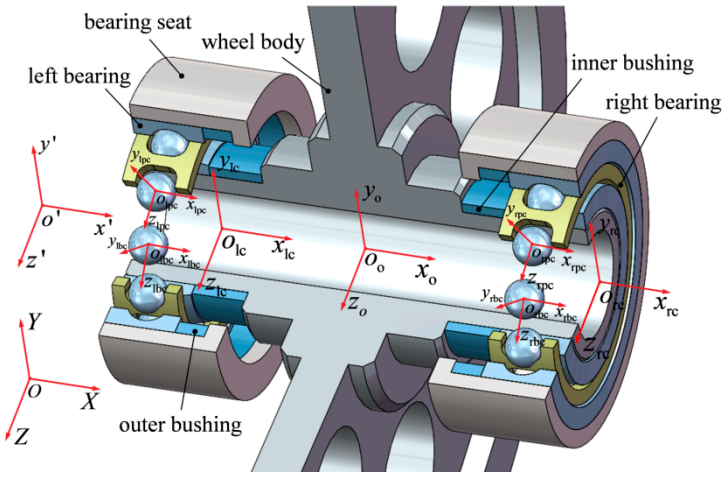

Figure 1. Coordinate system of CMGB.

(1) The inertial coordinate system $\{O; Z, Y, Z\}$ is fixed relative to space.

(2) The reference coordinate system $\{o'; x', y', z'\}$ is known as the frame coordinate system. The axis x' is along the axial direction of the shaft system. The coordinate system, the outer rings of the bearings on both sides, and the body's frame are fixed. They can rotate with the frame. The bearing parts' state of motion can be analyzed through the reference coordinate system.

(3) The coordinate system of the inner ring is $\{o_o; x_o, y_o, z_o\}$. The origin coincides with the center of the shaft system, and the axis x_o coincides with the rotation axis of the inner ring.

(4) The coordinate system of the cage center of bearings is $\{o_{kc}; x_{kc}, y_{kc}, z_{kc}\}$ (l represents the left side, and r represents the right side for the subscript k). The origin coincides with the mass center of the cage, and the axis x_{kc} coincides with the rotation axis of the cage.

(5) The coordinate system of the cage pocket center is $\{o_{kpj}; x_{kpj}, y_{kpj}, z_{kpj}\}$. The coordinate origin coincides with the jth pocket center of the cage on the k side, y_{kpj} along the radial direction of the cage, z_{kpj} along the circumferential direction of the cage, and x_{kpj} along the axial direction of the bearing.

(6) The coordinate system of the steel ball center is $\{o_{kbj}; x_{kbj}, y_{kbj}, z_{kbj}\}$. The coordinate origin coincides with the jth steel ball center of the bearing on the k side, y_{kbj} along the radial direction of the bearing, z_{kbj} along the circumferential direction of the bearing, and x_{kbj} along the axial direction of the bearing.

2.2. Dynamic Differential Equations for CMGB

Firstly, the mathematical model of interaction forces and nonlinear dynamic differential equations of bearing were established, and the friction contact state of bearing under the micro-lubrication is considered. Then, the predictive-corrective GSTIFF (gear stiff) variable-step integration algorithm (refer to reference [35]) is adopted to solve the dynamic differential equations, and the dynamic characteristics and friction torque of the control moment gyroscope bearings under variable torque load conditions were investigated.

2.2.1. Force Analysis of CMGB

During the operation of the control moment gyroscope, assuming that the angular momentums of the spacecraft body and the high-speed rotor are H_S and H_R, a total angular momentum H_T for the spacecraft can be written as

$$H_T = H_S + H_R \tag{1}$$

The rotation of the control moment gyroscope frame causes changes in the direction of the high-speed rotor spin axis and the angular momentum H_R of the rotor, so the angular momentum H_S of the body will change to keep the total angular momentum H_T of the spacecraft unchanged.

As shown in Figure 2, by adjusting the length difference between the inner and outer bushing, the axial force is applied to the inner ring to complete the constant pressure preloading of the bearing. G_i is the gravity of the inner ring; q_i is the tilt angle of the inner ring; and L is the distance between the two centers of bearings on both sides. Let the rotational angular velocity of the control moment gyroscope frame relative to the inertial coordinate system be w' and the rotor's angular velocity be w_i, so the external moment M_S acting on the body can be written as

$$M_S = \frac{dH_S}{dt} = \frac{dH_T}{dt} - \frac{dH_R}{dt} \tag{2}$$

When the spacecraft adjusts its attitude, the frame of the control moment gyroscope rotates to change the direction of the rotation axis of the wheel body. Based on the conservation of angular momentum, the control moment gyro outputs an effective moment. At the same time, the inner ring of the bearing will bear the gyroscopic moment M_y and M_z produced by the wheel body based on the relationship between the action and reaction, which is equivalent to applying a moment to the axial plane of the bearing's inner ring and generating the centrifugal forces, $F_{cy'}$ and $F_{cx'}$, simultaneously.

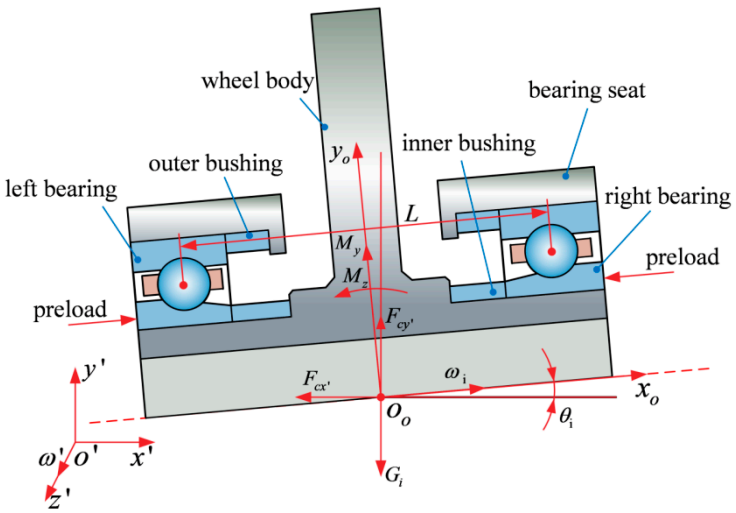

Figure 2. Force analysis of CMGB.

2.2.2. Dynamic Differential Equations of CMGB

Since the support bearings at both ends of the control moment gyroscope are working in the same state, the left bearing is an example of this research. The forces loading on the *j*th ball are shown in Figure 3.

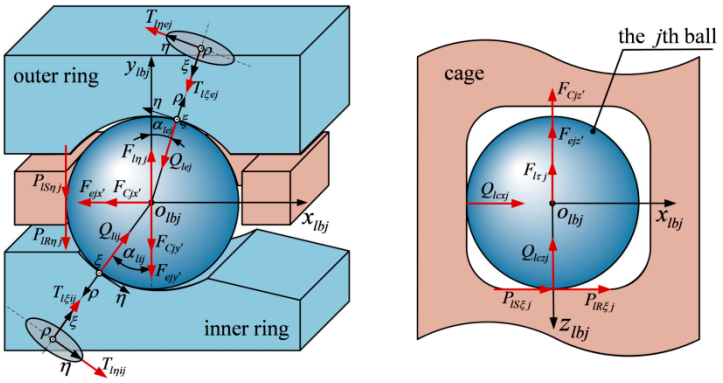

Figure 3. Forces loading on the *j*th ball.

In Figure 3, Subscripts *i* and *e* indicate the inner and outer raceway. The subscript *j* denotes the *j*th ball. *h* and *x* are the long and short axes of the contact ellipse between the ball and the raceway. Q_{lij} and Q_{iej} are the normal contact loads between the *j*th ball and raceway. T_{lhej}, T_{lhij}, T_{lxej}, and T_{lxij} are the drag forces in the contact area for the *j*th ball and the grooves. Q_{lczj} and Q_{lcxj} are the normal contact loads between the *j*th ball and cage in the tangential and axial directions. F_{lhj} and F_{ltj} are the components of the inertial force acting on the *j*th ball. P_{lRhj} and P_{lRxj} are the rolling frictional drag acting on the *j*th ball. P_{lShj} and P_{lSxj} are the sliding frictional drag acting on the *j*th ball. $F_{Cjx'}$, $F_{Cjy'}$, and $F_{Cjz'}$ are the convected inertial forces acting on the *j*th ball. $F_{ejx'}$, $F_{ejy'}$, and $F_{ejz'}$ are the Coriolis inertia forces acting on the *j*th ball.

The dynamic differential equations of the *j*th ball in the inertial coordinate system {*O*; *X*, *Y*, *Z*} are shown as

$$\begin{cases} m_{lb}\ddot{x}_{lbj} = Q_{lij}\sin\alpha_{lij} - Q_{lej}\sin\alpha_{lej} + T_{l\eta ij}\cos\alpha_{lij} - T_{l\eta ej}\cos\alpha_{lej} + P_{lS\xi j} + P_{lR\xi j} - Q_{lcxj} - F_{Cjx'} - F_{ejx'} \\ m_{lb}\ddot{y}_{lbj} = Q_{lij}\cos\alpha_{lij} - Q_{lej}\cos\alpha_{lej} - T_{l\eta ij}\sin\alpha_{lij} + T_{l\eta ej}\sin\alpha_{lej} + F_{l\eta j} - P_{lS\eta j} - P_{lR\eta j} - F_{Cjy'} - F_{ejy'} \\ m_{lb}\ddot{z}_{lbj} = T_{l\xi ej} - T_{l\xi ij} + Q_{lczj} - F_{l\tau j} - F_{Cjz'} - F_{ejz'} \\ J_{lx}\dot{\omega}_{lbxj} = T_{l\xi ej}\frac{D_w}{2}\cos\alpha_{lej} + T_{l\xi ij}\frac{D_w}{2}\cos\alpha_{lij} - \left(P_{lS\eta j} + P_{lR\eta j}\right)\frac{D_w}{2} - M'_{gx} \\ J_{ly}\dot{\omega}_{lbyj} = -T_{l\xi ej}\frac{D_w}{2}\sin\alpha_{lej} - T_{l\xi ij}\frac{D_w}{2}\sin\alpha_{lij} - G_{lyj} - \left(P_{lS\xi j} + P_{lR\xi j}\right)\frac{D_w}{2} - M'_{gy} \\ J_{lz}\dot{\omega}_{lbzj} = \left(T_{l\eta ej} + T_{l\eta ij}\right)\frac{D_w}{2} - G_{lzj} - M'_{gz} \end{cases} \quad (3)$$

The dynamic differential equations of the inner ring in the inertial coordinate system {*O*; *X*, *Y*, *Z*} are shown as

$$
\begin{cases}
m_i\ddot{x}_i = \sum\limits_{j=1}^{Z}\left(Q_{lij}\sin\alpha_{lij} - Q_{rij}\sin\alpha_{rij} + T_{l\eta ij}\cos\alpha_{lij} - T_{r\eta ij}\cos\alpha_{rij}\right) - F_{cx'} \\
m_i\ddot{y}_i = \sum\limits_{j=1}^{Z}\left[\begin{array}{l}\left(Q_{lij}\cos\alpha_{lij} - T_{l\eta ij}\sin\alpha_{lij}\right)\cos\varphi_{lj} + T_{l\xi ij}\sin\varphi_{lj} \\ +\left(Q_{rij}\cos\alpha_{rij} - T_{r\eta ij}\sin\alpha_{rij}\right)\cos\varphi_{rj} + T_{r\xi ij}\sin\varphi_{rj}\end{array}\right] + F_{cy'} \\
m_i\ddot{z}_i = \sum\limits_{j=1}^{Z}\left[\begin{array}{l}\left(Q_{lij}\cos\alpha_{lij} - T_{l\eta ij}\sin\alpha_{lij}\right)\sin\varphi_{lj} + T_{l\xi ij}\cos\varphi_{lj} \\ +\left(Q_{rij}\cos\alpha_{rij} - T_{r\eta ij}\sin\alpha_{rij}\right)\sin\varphi_{rj} + T_{r\xi ij}\cos\varphi_{rj}\end{array}\right] + F_{cz'} \\
I_{iy}\dot{\omega}_{iy} - (I_{iz} - I_{ix})\omega_{iz}\omega_{ix} = M_y + \\
\sum\limits_{j=1}^{Z}\left[\begin{array}{l}\left(0.5d_{lmj} + 0.5D_w f_i\cos\alpha_{lij}\right)\left[\left(\begin{array}{l}Q_{lij}\sin\alpha_{lij} \\ +T_{l\eta ij}\cos\alpha_{lij}\end{array}\right)\sin\varphi_{lj} - \left(\begin{array}{l}Q_{rij}\sin\alpha_{rij} \\ -T_{r\eta ij}\cos\alpha_{rij}\end{array}\right)\sin\varphi_{rj}\right] \\ +0.5L\left[\left(Q_{lij}\cos\alpha_{lij} + T_{l\eta ij}\sin\alpha_{lij}\right)\sin\varphi_{lj} - \left(Q_{rij}\cos\alpha_{rij} + T_{r\eta ij}\sin\alpha_{rij}\right)\sin\varphi_{rj}\right] \\ +0.5\left(L - D_w f_i\sin\alpha_{lij}\right)T_{l\xi ij}\cos\varphi_{lj} - 0.5\left(L - D_w f_i\sin\alpha_{rij}\right)T_{r\xi ij}\cos\varphi_{rj}\end{array}\right] \\
I_{iz}\dot{\omega}_{iz} - \left(I_{ix} - I_{iy}\right)\omega_{ix}\omega_{iy} = M_z + \\
\sum\limits_{j=1}^{Z}\left[\begin{array}{l}\left(0.5d_{lmj} + 0.5D_w f_i\cos\alpha_{lij}\right)\left[\left(\begin{array}{l}Q_{lij}\sin\alpha_{lij} \\ +T_{l\eta ij}\cos\alpha_{lij}\end{array}\right)\cos\varphi_{lj} - \left(\begin{array}{l}Q_{rij}\sin\alpha_{rij} \\ -T_{r\eta ij}\cos\alpha_{rij}\end{array}\right)\cos\varphi_{rj}\right] \\ +0.5L\left[\left(Q_{lij}\cos\alpha_{lij} + T_{l\eta ij}\sin\alpha_{lij}\right)\cos\varphi_{lj} - \left(Q_{rij}\cos\alpha_{rij} + T_{r\eta ij}\sin\alpha_{rij}\right)\cos\varphi_{rj}\right] \\ +0.5\left(L - D_w f_i\sin\alpha_{lij}\right)T_{l\xi ij}\sin\varphi_{lj} - 0.5\left(L - D_w f_i\sin\alpha_{rij}\right)T_{r\xi ij}\sin\varphi_{rj}\end{array}\right]
\end{cases}
\tag{4}
$$

In the above equations, J_{lx}, J_{ly}, and J_{lz} are the inertia moments of the ball along three coordinate axes in the coordinate system $\{o_{lbj}; x_{lbj}, y_{lbj}, z_{lbj}\}$; G_{lyj} and G_{lzj} are the inertia moments of the ball in the y_{lbj} and z_{lbj} directions; $F_{cx'}$, $F_{cy'}$, and $F_{cx'}$ are the centrifugal force caused by the torque applied to the inner ring; w_{lxj}, w_{lyj}, and w_{lzj} are the components of the angular velocity of the ball in the x_{lbj}, y_{lbj}, and z_{lbj} directions; $\dot{\omega}_{lxj}$, $\dot{\omega}_{lyj}$, and $\dot{\omega}_{lzj}$ is the angular acceleration components of the ball in the x_{lbj}, y_{lbj}, and z_{lbj} directions; $\ddot{x}_i$, $\ddot{y}_I$, and $\ddot{z}_i$ are the accelerations of the inner ring mass center; I_{ix}, I_{iy}, and I_{iz} are the inertia moments of the inner ring; w_{ix}, w_{iy}, and w_{iz} are the angular velocities of the inner ring; $\dot{\omega}_{iy}$ and $\dot{\omega}_{iz}$ are the angular accelerations of the inner ring; and f_i is the groove curvature radius coefficient of the inner ring.

Figure 4 shows the force analysis for the cage. d_z and d_x are the tangential and axial movements of the ball relative to the pocket center; b_p is the width of the cage pocket; R is the ball radius. e is the cage eccentricity; Dy'_c and Dz'_c are the two components of the eccentricity; j_c is the azimuth angle of the cage; j_{lj} is the azimuth angle of the jth ball; h_o is the minimum oil film thickness between the cage and the outer ring guide surface; F'_{lcQ}, F'_{lct}, and M'_{lcx} are the normal and tangential forces and moments acting on the cage by the guide rib; F_{lcxj} is the axial friction force of the guide ring on the cage when they contact; Q'_{lczj} is the normal force between the ball and the cage pocket in the direction of motion; Q'_{lcxj} is the axial force between the ball and the cage pocket; F_{lcxj} and F_{lcxj} are the axial and radial components of the friction force between the ball and the cage pocket; G_{lc} is the cage gravity; w_{lc} is the angular velocity of the cage in the reference coordinate system $\{o'; x', y', z'\}$.

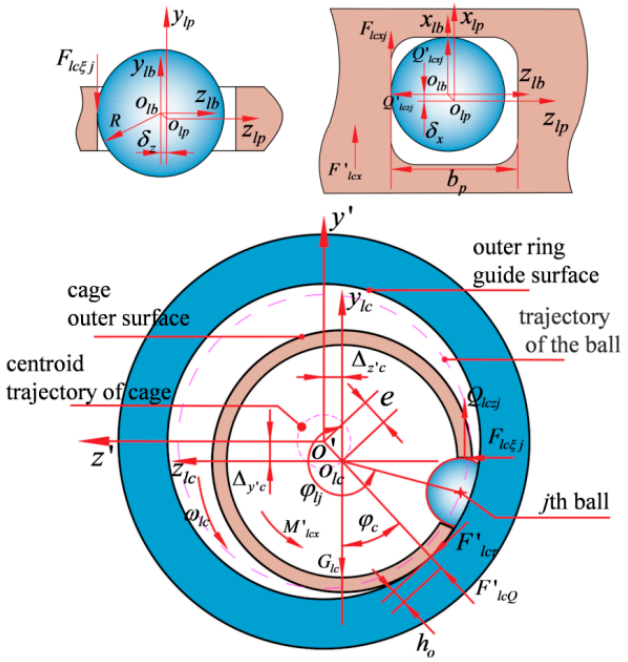

Figure 4. Forces loading on the cage.

The dynamic differential equations for the cage in the inertial system $\{O; X, Y, Z\}$ are shown as

$$\begin{cases} m_{lc}\ddot{x}_{lcx} = F_{Ccx'} + F_{ecx'} + \sum_{j=1}^{Z}\left(Q'_{lcxj} + F_{lcxj}\right) \\ m_{lc}\ddot{y}_{lcy} = F'_{lc\tau}\sin\varphi_c + F'_{lcQ}\cos\varphi_c + \sum_{j=1}^{Z}\left[F_{lc\xi j}\cos\varphi_{lj} - Q_{lczj}\sin\varphi_{lj}\right] - F_{Ccy'} - F_{ecy'} - G_{lc} \\ m_{lc}\ddot{z}_{lcz} = F'_{lc\tau}\cos\varphi_c - F'_{lcQ}\sin\varphi_c + \sum_{j=1}^{Z}\left[F_{lc\xi j}\sin\varphi_{lj} + Q_{lczj}\cos\varphi_{lj}\right] + F_{Ccz'} + F_{ecz'} \\ I_{lcx}\dot{\omega}_{lcx} - \left(I_{lcy} - I_{lcz}\right)\omega_{lcy}\omega_{lcz} = \sum_{j=1}^{Z}\left[Q_{lczj}\frac{d_{mj}}{2}\right] + M'_{lcx} \\ I_{lcy}\dot{\omega}_{lcy} - (I_{lcz} - I_{lcx})\omega_{lcz}\omega_{lcx} = \sum_{j=1}^{Z}\left[\left(Q'_{lcxj} + F_{lcxj}\right)\frac{d_{mj}}{2}\sin\varphi_j\right] + F'_{lcx}\frac{D_{c2}}{2}\sin\varphi_c + M_{gcy} \\ I_{lcz}\dot{\omega}_{lcz} - \left(I_{lcx} - I_{lcy}\right)\omega_{lcx}\omega_{lcy} = \sum_{j=1}^{Z}\left[\left(Q'_{lcxj} + F_{lcxj}\right)\frac{d_{mj}}{2}\cos\varphi_j\right] + F'_{lcx}\frac{D_{c2}}{2}\cos\varphi_c + M_{gcz} \end{cases} \quad (5)$$

where m_{lc} is the quality of the cage; $\ddot{x}_{lcx}$, $\ddot{y}_{lcy}$, and $\ddot{z}_{lcz}$ are the accelerations of the cage center-of-mass; I_{lcx}, I_{lcy}, and I_{lcz} are the moment of inertia of the cage; M_{gcy} and M_{gcz} are the components of the gyroscopic moments acting on the cage in the y and z directions; $F_{Ccz'}$, $F_{Ccy'}$, $F_{Ccx'}$, $F_{ecz'}$, $F_{ecy'}$, and $F_{ecx'}$ are the components of the Coriolis inertia forces and the convected inertial forces acting on the cage in the non-inertial coordinate system, respectively; $\dot{\omega}_{lcx}$, $\dot{\omega}_{lcy}$, and $\dot{\omega}_{lcz}$ is the angular acceleration of the cage; Z is the number of balls; d_{mj} is the pitch diameter of the ball.

3. Results and Discussion

A control moment gyroscope is supported by a pair of B7005 angular contact ball bearings. The main parameters of bearing are shown in Table 1.

Table 1. The main structural parameters of B7005 bearing.

Item	Value
Bearing inner diameter (mm)	25
Bearing outer diameter (mm)	47
Bearing width (mm)	12
Ball diameter (mm)	6.35
Cage outer diameter (mm)	39.26
Material of inner ring, outer ring, ball	9Cr18Mo
Material of cage	Porous polyimide
Lubricating oil	4129 aviation lubricating oil

3.1. Dynamic Characteristics and Friction Torque of Bearing under the Steady-State Condition

When the control moment gyroscope works in the steady state, it does not output the moment, the speed of the inner ring is 9500 r/min, the axial preload is 110 N, the working temperature is 30 °C, and the moment is 0 N·m. The results are as follows.

In Figures 5–9, it can be seen that when the bearing is working under the steady-state condition, the collision forces between the balls and cage are small, and the maximum collision force is 0.98 N. The speed of the cage remains at around 3942.9 r/min with a fluctuation amplitude of ±21.1 r/min. The friction torque of the bearing remains at around 3.6 N·mm with a maximum fluctuation amplitude of 0.07 N·mm, and it was noted that the friction torque fluctuation between balls and cage is the primary cause for the friction torque fluctuation of bearing, this has been proven in refs. [25,33]. As the cage is affected by gravity, its mass center shifts 0.1 mm downwards and then moves irregularly within a small range. The ball moves around 6.398 mm in the x-axis direction with a range of 0.64 μm.

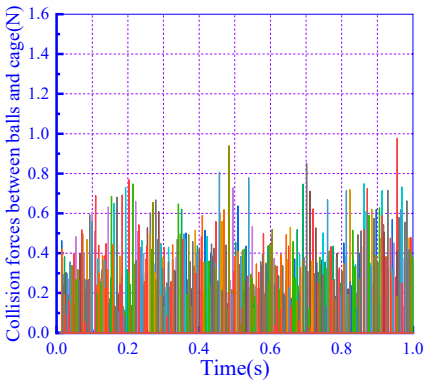

Figure 5. Collision forces between balls and cage.

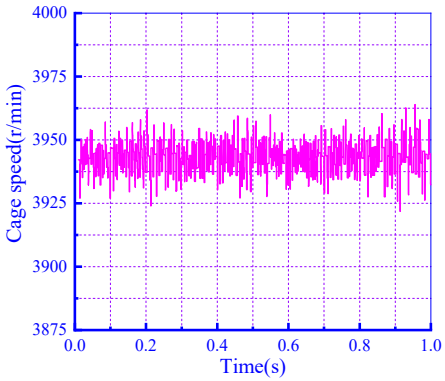

Figure 6. Cage speed.

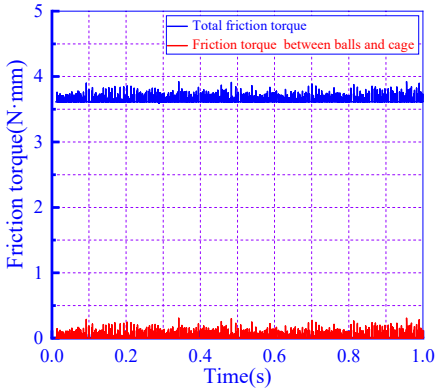

Figure 7. Friction torque of bearing.

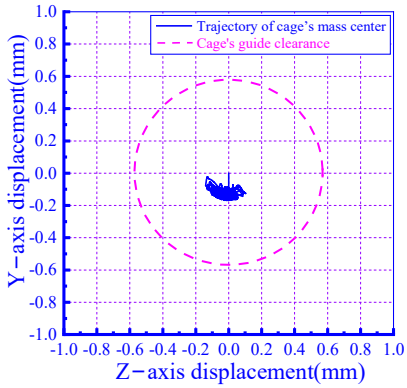

Figure 8. Trajectory of cage's mass center.

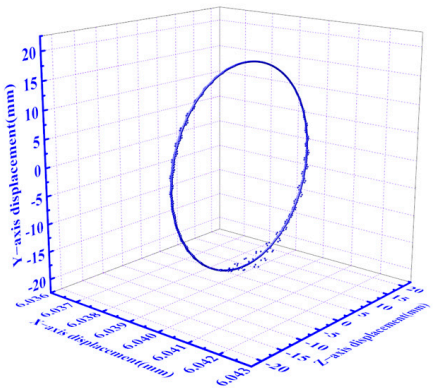

Figure 9. Ball's trajectory.

When the control moment gyroscope does not output the moment, the bearings at both sides do not bear the corresponding moment. At this time, it can be seen from Figures 5 and 7 that the friction torque fluctuation of the bearing is related to the collision and friction between balls and cage.

3.2. Dynamic Characteristics and Friction Torque of Bearing under the Condition of the Time-Varying Moment

The control moment gyroscope outputs the moment through the rotating frame. The bearing bears the corresponding gyroscopic moment, which has different response times under the other working conditions, such as the inner ring of the bearing being subjected to a variable moment of 125 N·m with response times of 0.2 s, 0.5 s, and 1.0 s, respectively, as shown in Figure 10.

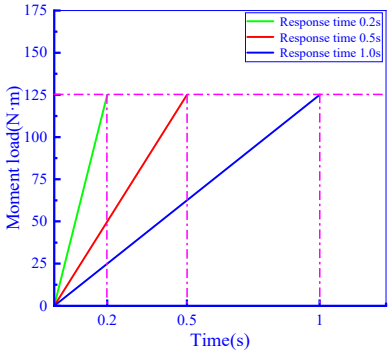

Figure 10. Time-varying moment of bearing.

The speed of the inner ring is 9500 r/min, the axial preload is 110 N, and the working temperature is 30 °C. The dynamic characteristics and friction torque of bearing under the time-varying moment are as follows.

It can be seen that the friction torque fluctuation of the bearing increases with the increase in the moment, and the growth rate increases first and then decreases. In Figures 11–13, when the moment rises to a critical value (around 62.5 N·m), the collision forces between the balls and cage increase, and the fluctuation amplitude of cage speed and the friction torque of the bearing also increase. Compared with the dynamic characteristics of bearings under the different response times, the shorter the response time, the greater the collision force between the balls and cage, and the greater the fluctuation amplitude of cage speed and friction torque. In Figures 14 and 15, referring to the trajectory of the cage's mass center and the ball's mass center, when the moment increases to a critical value (around 62.5 N·m), the trajectory of the cage's mass center changes from a small range of irregular movement into the divergent circular vortex, and the axial displacement of the balls increases.

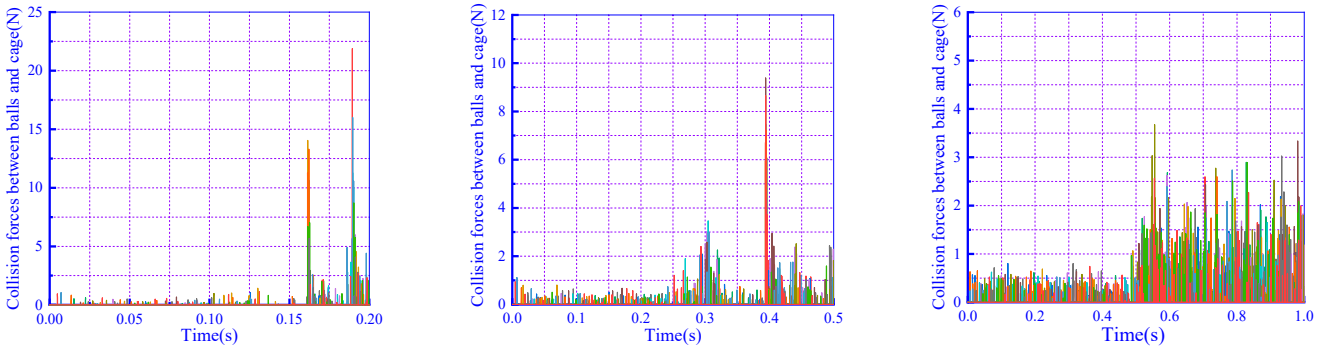

(**a**) 0.2 s (**b**) 0.5 s (**c**) 1.0 s

Figure 11. Collision force between balls and cage under the different response times.

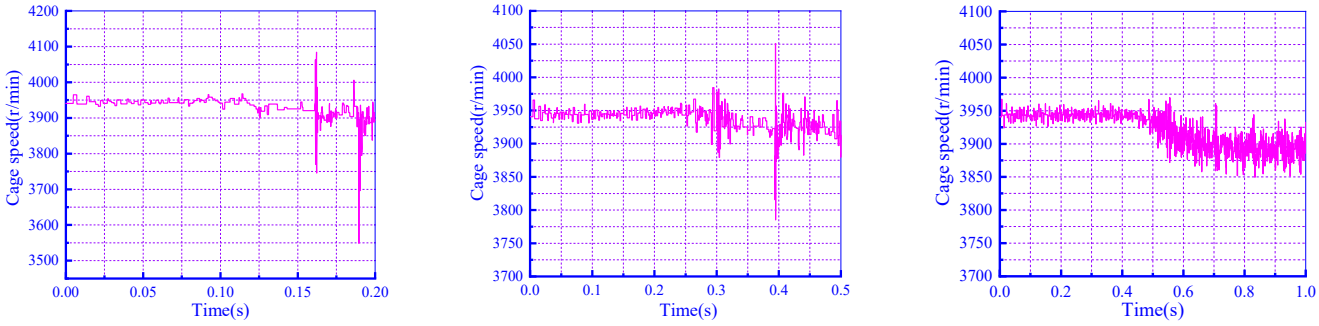

(**a**) 0.2 s (**b**) 0.5 s (**c**) 1.0 s

Figure 12. Cage speed under the different response times.

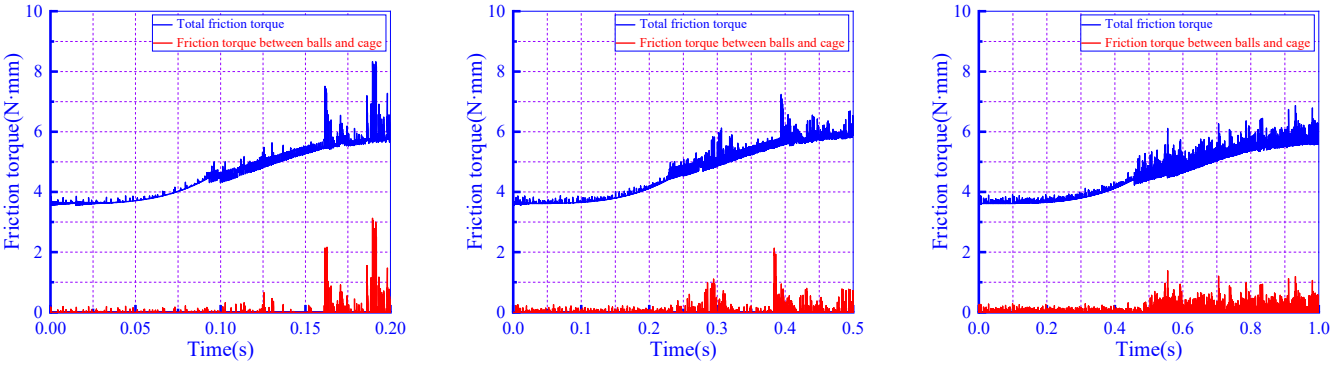

(**a**) 0.2 s (**b**) 0.5 s (**c**) 1.0 s

Figure 13. Friction torque fluctuation of bearing under the different response times.

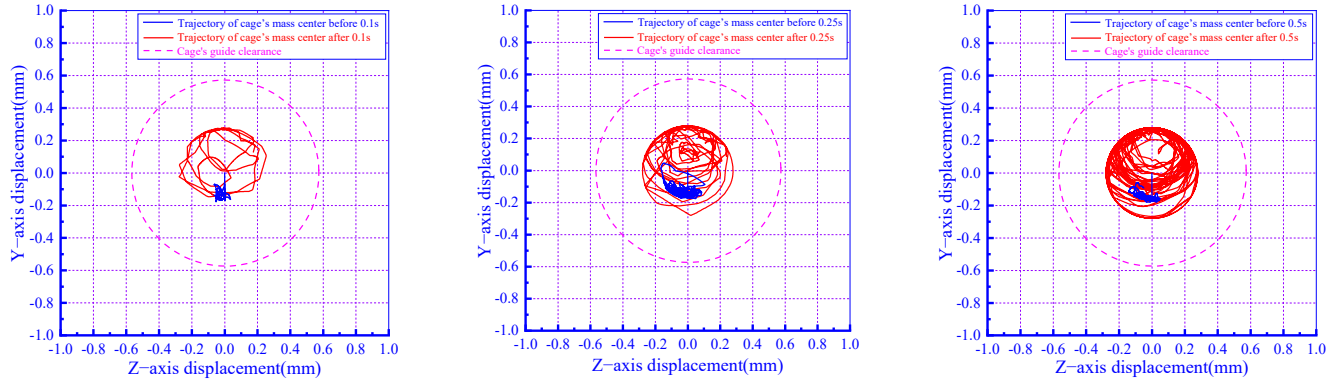

(**a**) 0.2 s (**b**) 0.5 s (**c**) 1.0 s

Figure 14. Trajectory of cage's mass center under the different response times.

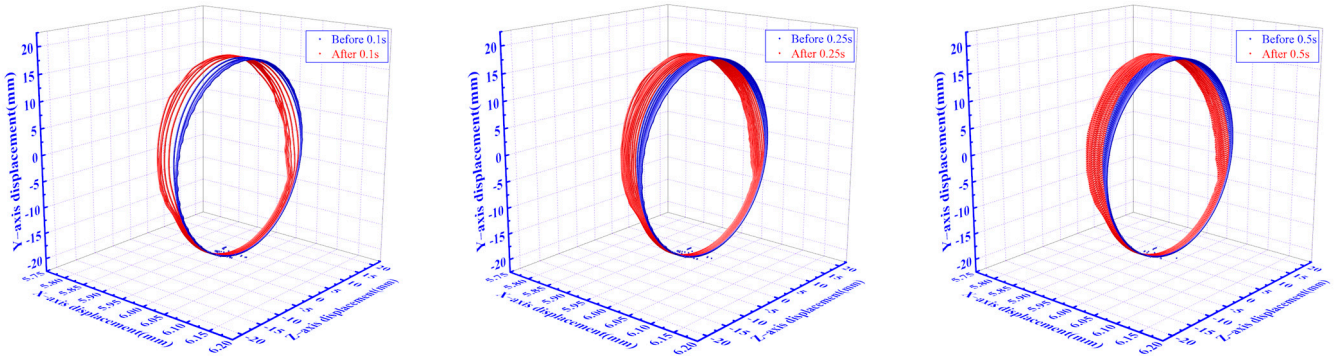

(**a**) 0.2 s (**b**) 0.5 s (**c**) 1.0 s

Figure 15. Ball's trajectories under the different response times.

To reveal the relationship between the friction torque fluctuation of the bearing and the motions of the cage and ball under the time-varying moment loading, the trajectories of the cage's mass center are extracted in the *Y* and *Z* direction, as shown in the following figures.

In Figure 16, when the moment reaches 62.5 N·m approximately, the motion amplitude of the cage's mass center in the *Y* and *Z* directions increases significantly, and the trajectory of the cage's mass center changes from a small range of irregular movement into the divergent circular vortex. Referring to Figure 13, the fluctuation amplitude of friction torque increases when the trajectory of the cage's mass center changes abruptly at 0.1 s. When the trajectory of the cage's mass center changes suddenly in the *Y* and *Z* directions, the axial displacement of the ball increases, which is related to the loading state of the ball.

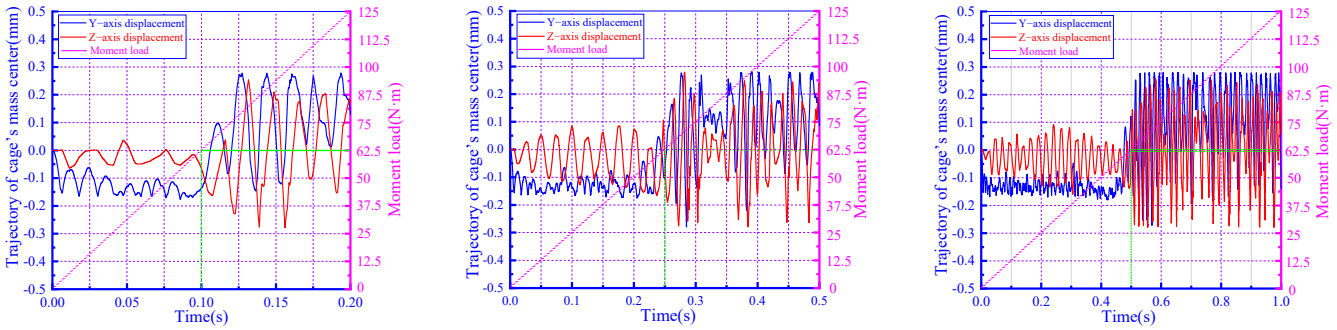

(**a**) 0.2 s (**b**) 0.5 s (**c**) 1.0 s

Figure 16. Trajectory of cage's mass center with different response times.

To further explore the reasons for the sudden change of bearing dynamic characteristics under time-varying moment loading, the forces between the ball and the inner raceway with a response time of 1.0s are extracted at different times of 0 s, 0.2 s, 0.4 s, 0.5 s, 0.6 s, 0.8 s, and 1.0 s, as shown in Figure 17.

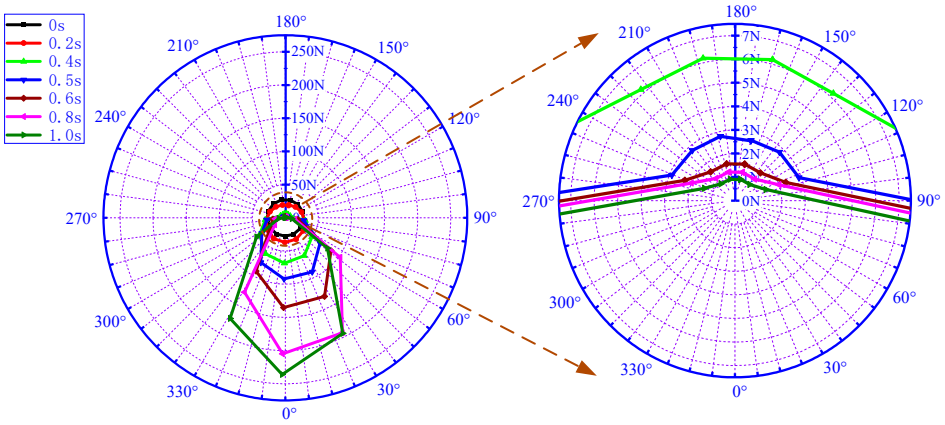

Figure 17. Loading conditions of the balls at different times.Loading conditions of the balls at different times are shown in Table 2.

Table 2. Loading forces of balls.

Time	0 s	0.2 s	0.4 s	0.5 s	0.6 s	0.8 s	1.0 s
Moment (N·mm)	0	25	50	62.5	75	100	125
Maximum force between balls and inner raceway (N)	27.79	36.92	68.49	95.99	135.22	204.85	235.92
Minimum force between balls and inner raceway (N)	27.63	19.17	6.19	2.63	1.60	1.24	0.92

Figure 17 and Table 2 show that the maximum force between the ball and the inner raceway increases from 27.79 N to 95.99 N in 0 s~0.5 s and from 95.99 N to 235.92 N in 0.5 s~1 s as the moment increases and the minimum force between balls and inner raceway decreases from 27.63 N to 0.92 N, which is less than 3 N after 0.5 s. By comparing the trajectory of the ball with a response time of 1.0 s in Figure 15, it can be seen that when the bearing is running, the maximum axial offset of the ball in the area with a large force between the ball and the inner raceway is 23 (±0.5) mm, and the maximum axial offset of the ball in the area with a small force between the ball and the inner raceway is 78 (±0.5) mm.

The main reason for the above phenomenon is that with the increase in the moment during bearing operation, the inner ring and outer ring produce a relative tilt, the non-uniformity of the force between the ball and the raceway increases, and the minimum force between the ball and the raceway decreases. When the minimum force between the ball

and the raceway decreases to a certain value (the moment reaches the critical value), the constraining force of the raceway on the ball is insufficient, and the gap between the ball and the raceway increases due to the inclination between the bearing inner ring and outer ring, resulting in a large axial offset of the ball and the collision force between balls and the cage is increased. The increase in the collision force between balls and the cage changes the state of force on the cage, resulting in increasing the cage speed fluctuations, and the trajectory of the cage's mass center changes from a small range of irregular movement to a divergent ring vortex, thus increasing the fluctuation amplitude of the bearing friction torque.

3.3. Effect of Preload on Dynamic Characteristics and Friction Torque of Bearing under the Condition of Time-Varying Moment

The speed of the inner ring is 9500 r/min, and the working temperature is 30 °C. The moment rises from 0 N·m to 125 N·m in 1.0 s. The bearing's dynamic characteristics and friction torque are analyzed when the axial preload is 60 N, 110 N, and 160 N, respectively. The results are as follows.

In Figures 18–20, it can be seen that under the time-varying moment, the preload force is 60 N, 110 N, and 160 N, and the bearing dynamic characteristics change when the simulation time is near 0.4 s, 0.5 s, and 0.55 s, respectively; that is, the collision forces between the balls and cage increases, the cage speed fluctuation amplitude increases, and the fluctuation amplitude of bearing friction torque increases. In Figures 21 and 22, the trajectory of the cage's mass center changes from a small range of irregular movement to a circular vortex, and the axial displacement of balls increases, at which time the critical torque load (50 N·m,62.5 N·m, and 68.75 N·m) is reached. In the process of torque increase, the increase in preload leads to the bearing friction torque increase, but the fluctuation amplitude of the friction torque is decreased, and the axial offset of the ball is decreased. To further analyze the influence of preload on bearing dynamic characteristics under the time-varying moments, the maximum and minimum axial displacements of balls under the different preloads were extracted, as shown in Table 3.

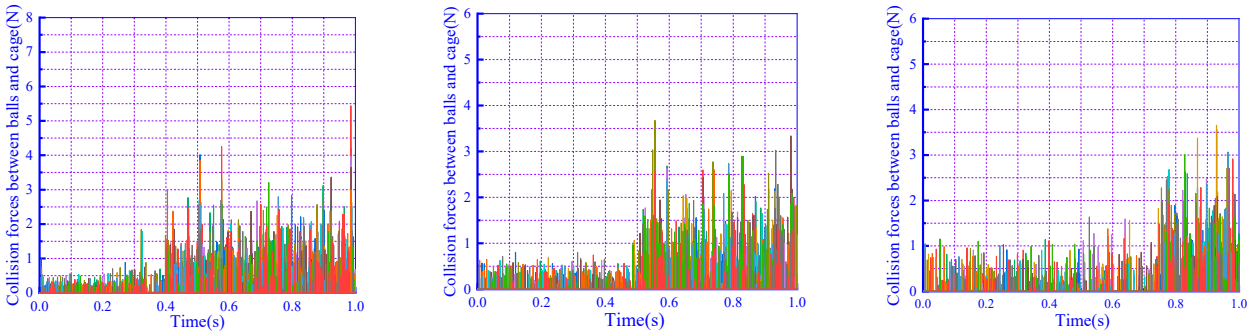

(**a**) 60 N (**b**) 110 N (**c**) 160 N

Figure 18. Collision force between balls and cage under the different preloads.

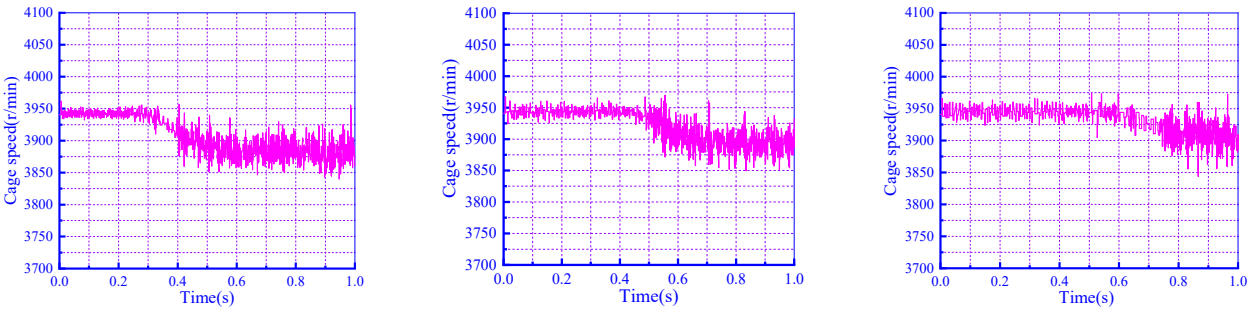

(**a**) 60 N (**b**) 110 N (**c**) 160 N

Figure 19. Cage speed under the different preloads.

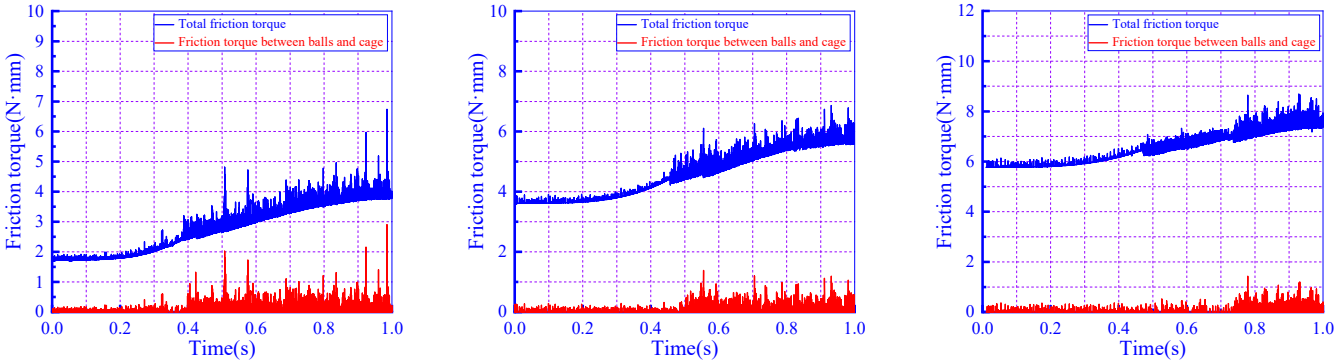

(**a**) 60 N (**b**) 110 N (**c**) 160 N

Figure 20. Friction torque fluctuation of bearing under the different preloads.

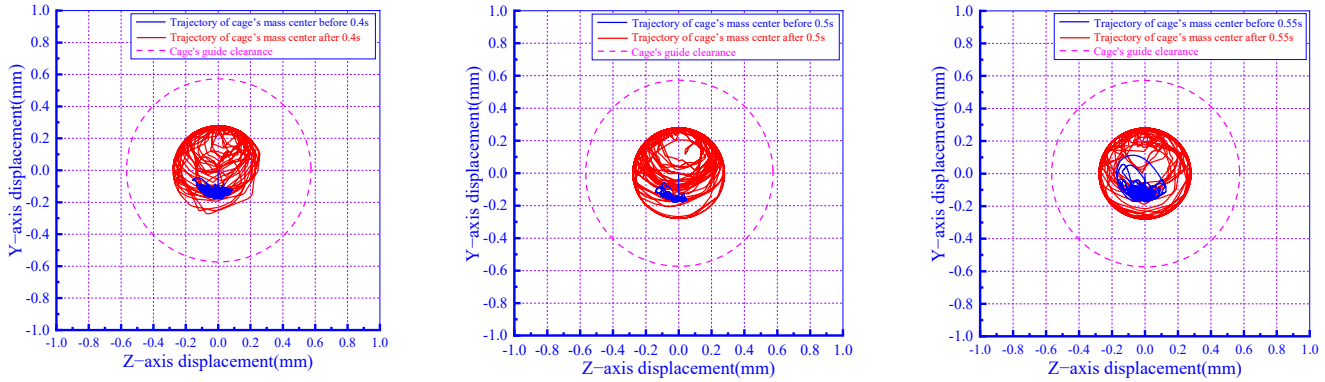

(**a**) 60 N (**b**) 110 N (**c**) 160 N

Figure 21. Trajectory of cage's mass center under the different preloads.

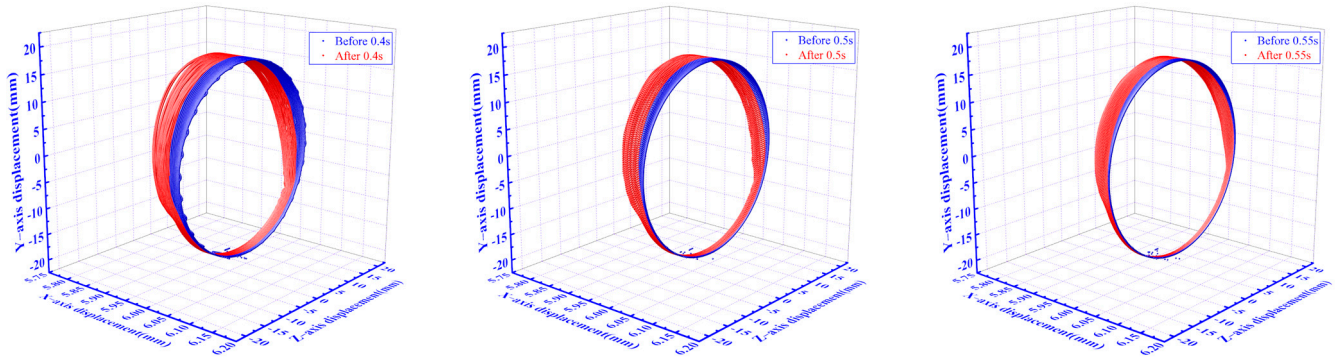

(a) 60 N (b) 110 N (c) 160 N

Figure 22. Ball's trajectories under the different preloads.

Table 3. Axial displacement of the ball.

Axial Preload (N)	60	110	160
Maximum axial displacement (μm)	90.3	78.2	50.9
Minimum axial displacement (μm)	25.1	23.5	9.1

As shown in Table 3, with the increase in preload under the condition of time-varying moment, the ball's maximum axial displacement and minimum axial displacement are reduced.

The contact forces between the balls and the inner raceway are analyzed under the different preloads when the bearing is activated by the time-varying moment, as shown in Figures 23–25.

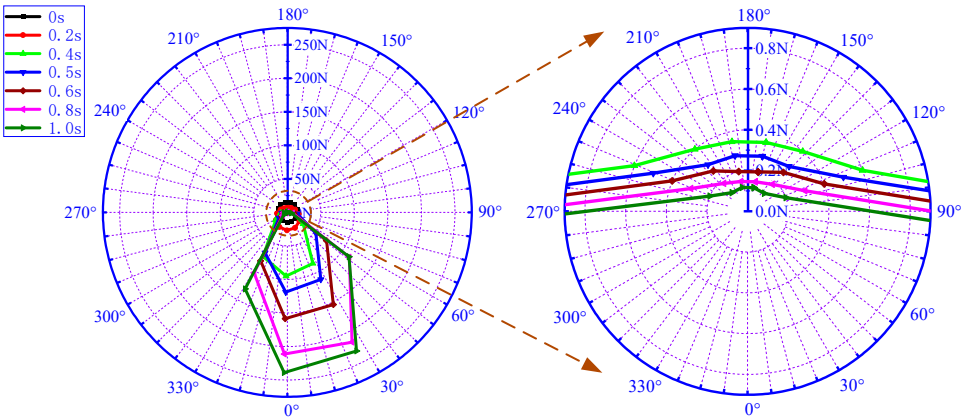

Figure 23. Ball's loading at 60 N preload.

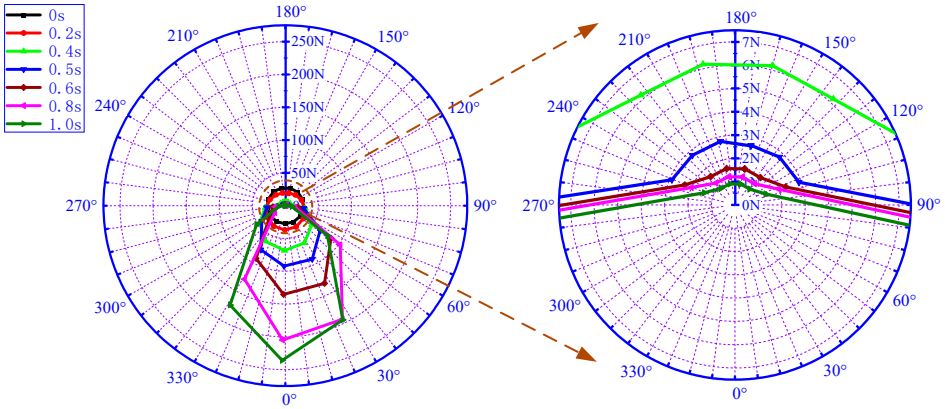

Figure 24. Ball's loading at 110 N preload.

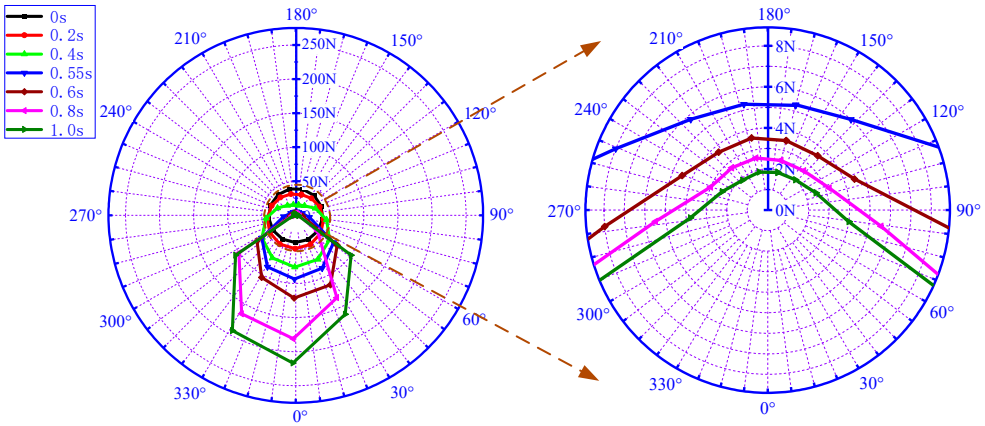

Figure 25. Ball's loading at 160 N preload.Therefore, under the time-varying moment, increasing the bearing preload can improve the bearing capacity to resist the time-varying moment and reduce the fluctuation amplitude of bearing friction torque.

The contact forces between the balls and the inner raceway under the critical moment are shown in Table 4.

Table 4. The ball's loading under the critical moment.

Axial Preload (N)	60	110	160
Time (s)	0.4	0.5	0.55
Critical moment (N·m)	50	62.5	68.75
Maximum force between the ball and inner raceway (N)	96.23	94.99	93.50
Minimum force between the ball and inner raceway (N)	0.35	2.63	5.28

It can be seen in Figures 23–25 and Table 4 that the increase in preload increases the critical moment of bearing with a sudden change in dynamic characteristics, increases the maximum contact force between the ball and the inner ring, decreases the minimum contact forces, and improves the bearing's ability to bear variable moment. Under the critical moment, with the increase in bearing preload, the minimum contact force between the ball and the inner ring increases, and the constraining force of the inner ring on the ball during bearing operation also increases, which reduces the axial displacement of the ball during operation, reduces the collision forces between the balls and cage, and increases the moment that the cage speed and the cage centroid trajectory can bear when the sudden change occurs. The increase in preload increases the friction between the ball and the raceway. Therefore, the bearing friction torque with a larger preload is also larger under the same conditions. The fluctuation amplitude of bearing friction torque decreases because the increase in preload reduces the axial displacement of the ball and then reduces the collision forces between the balls and cage, and the collision between the ball and cage is the main reason for the fluctuation of bearing friction torque.

3.4. Effect of Working Temperature on Dynamic Characteristics and Friction Torque of Bearings under the Time-Varying Moment

The speed of the inner ring is 9500 r/min, and the axial preload is 110 N. The moment rises from 0 N·m to 125 N·m in 1.0 s. When the working temperature is 0 °C, 30 °C, and 60 °C, the results are shown as follows.

In Figures 26–30, it can be seen that no matter whether the temperature is 0 °C, 30 °C, or 60 °C, the motion states of the cage and balls change suddenly when the moment reaches 62.5 N·m near 0.5 s, named the critical moment. After the moment exceeds the critical moment of 62.5 N·m, the collision forces between the balls and cage decrease with the temperature increase. The cage speed fluctuation amplitude decreases, and the bearing friction torque's fluctuation amplitude decreases. The dispersion of the cage circular vortex reduces. The main reason is that with the increase in temperature, the lubricant viscosity decreases, and then the oil sling rate of the porous oil-containing cage increases, which leads to a larger amount of oil in the contact surfaces of the bearing. The decrease in friction coefficient between contact surfaces will reduce cage speed and bearing friction torque fluctuation.

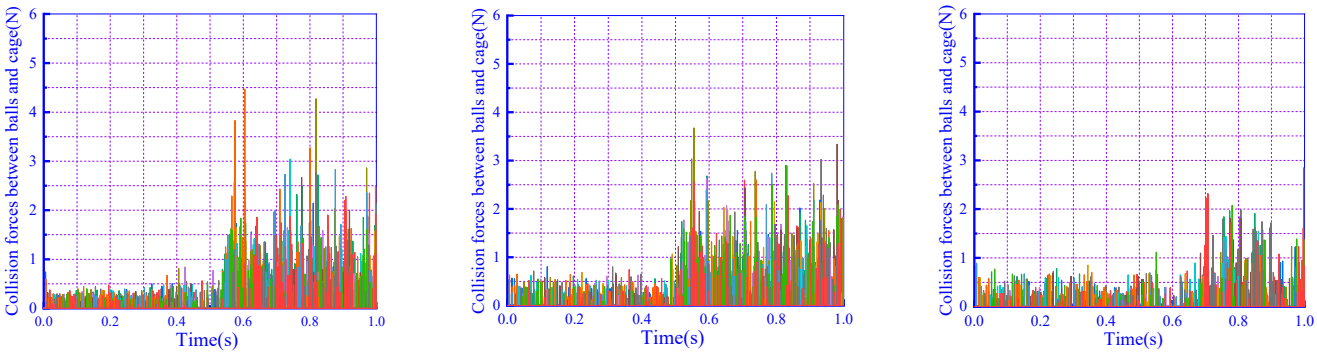

(**a**) 0 °C (**b**) 30 °C (**c**) 60 °C

Figure 26. Collision force between balls and cage under the different working temperatures.

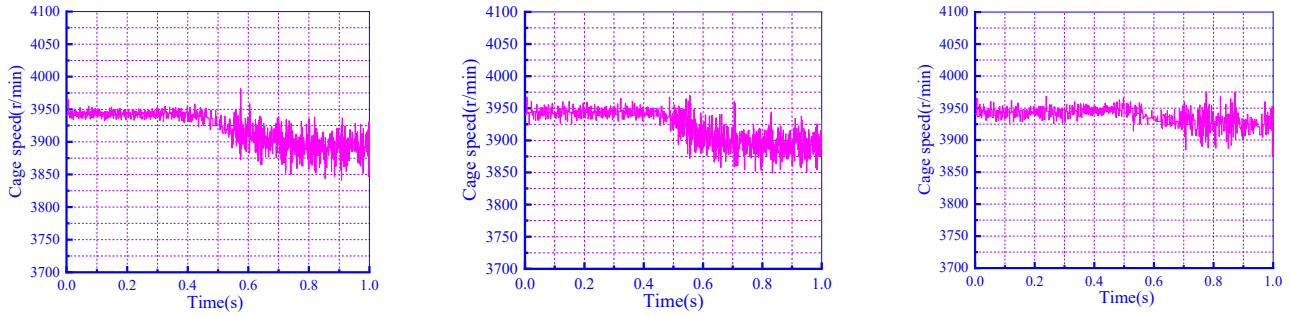

(**a**) 0 °C (**b**) 30 °C (**c**) 60 °C

Figure 27. Cage speed under the different working temperatures.

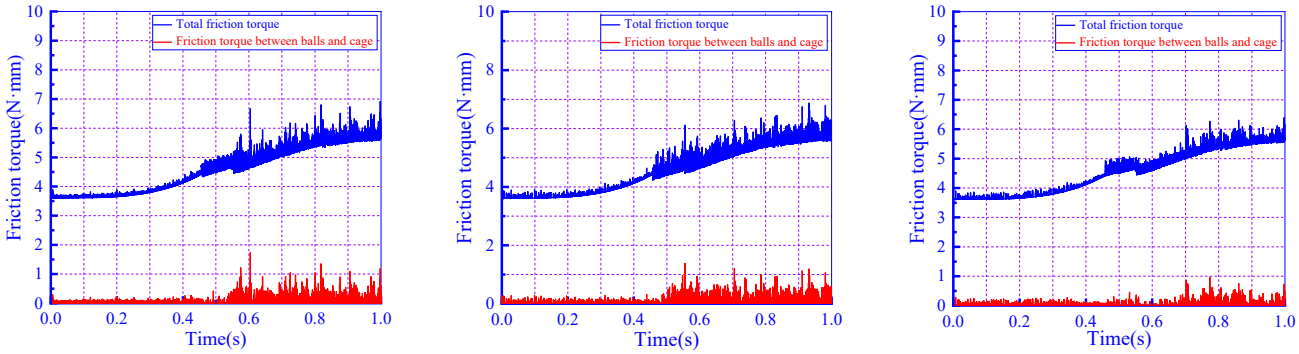

(**a**) 0 °C (**b**) 30 °C (**c**) 60 °C

Figure 28. Friction torque fluctuation of bearing under the different working temperatures.

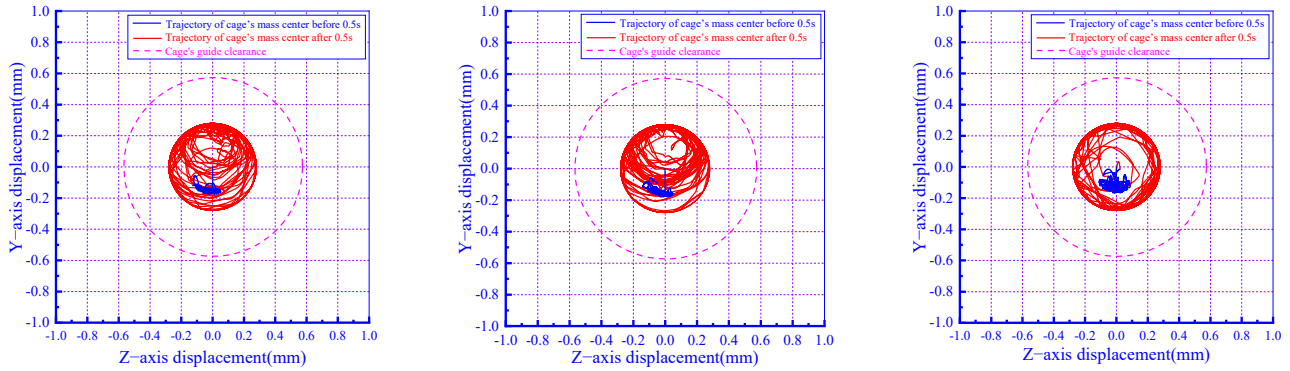

(**a**) 0 °C (**b**) 30 °C (**c**) 60 °C

Figure 29. Trajectory of cage's mass center under the different working temperatures.

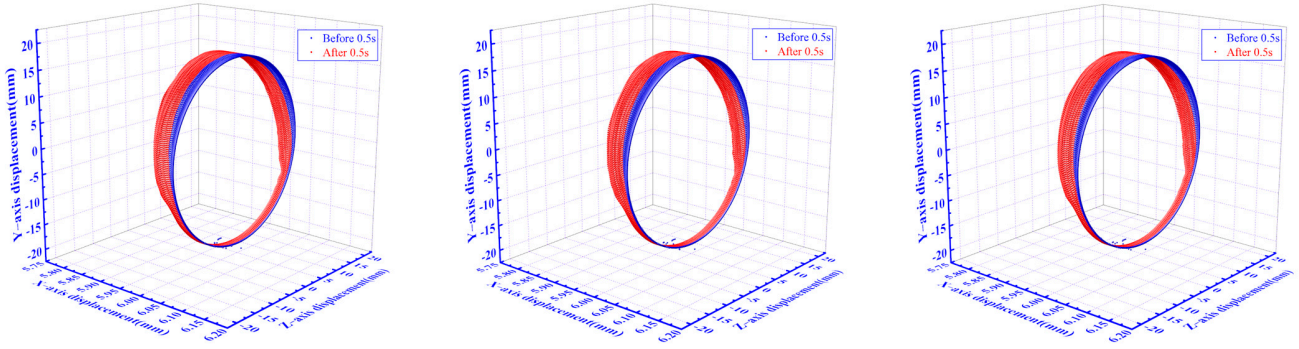

(**a**) 0 °C (**b**) 30 °C (**c**) 60 °C

Figure 30. Ball's trajectories under the different working temperatures.

3.5. Experimental Verification

Experiments were performed on a rotary table test for the control moment gyroscope assembly under the time-varying moment, as shown in Figure 31. This experiment simulated the rotation of the frame in the control moment gyroscope by adjusting the rotation of the rotary table. When the gyroscope is running, the wheel body rotates at a high speed, and the rotation axis of the wheel body changes when the rotating table rotates. The wheel will output the corresponding gyroscopic moment, which is related to the moment of inertia of the wheel body, the rotation speed of the wheel body, and the rotation speed of the rotating table. The faster the rotation speed of the rotating table, the faster the rotation axis of the wheel body will change, and the greater the external output gyroscopic moment. Right now, the angular contact ball bearing supporting the rotation of the wheel body will bear the response torque load.

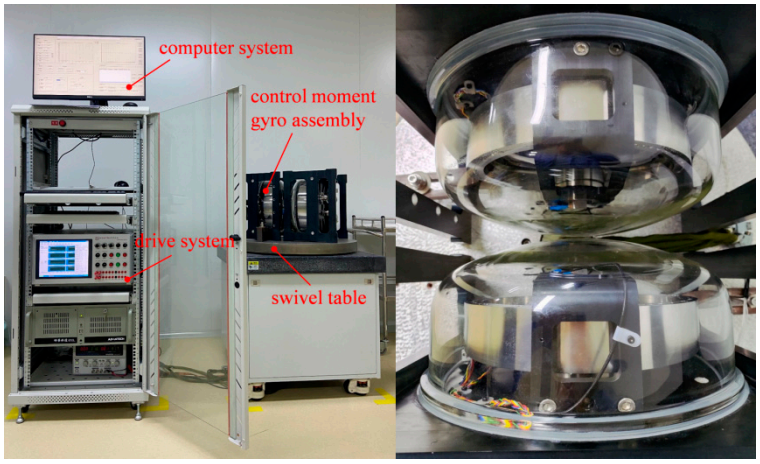

Figure 31. Table test of control moment gyroscope.

The support bearings at both ends of the control moment gyro rotor are B7005 angular contact ball bearings with an axial preload of 110 N. The experimental environment temperature is 25 °C, and the drive system is used to control the rotation speed of the wheel body at 8000 r/min. The computer system adjusts the turntable to uniformly accelerate from 0°/s to a fixed rotation speed at different angular accelerations. The angular acceleration of the turntable rotation is different, and the time it takes to reach the fixed rotation speed is also different, which means the response time of the gyroscopic torque output to the outside is different. The computer system controls the turntable speed to uniformly accelerate from 0°/s to 60°/s at acceleration levels of 0.01°/s^2, 0.05°/s^2, and 0.1°/s^2, as shown in Figure 32. At this time, the response times of the bearings at both ends are 100 min, 20 min, and 10 min, respectively, bearing the varying torque load from 0 N·m to 125 N·m. During this process, the drive system that rotates the wheel body keeps the voltage at both ends of the drive motor constant, collects the current change signal, and determines the change in friction torque of the CMGB based on the linear proportional relationship between friction torque and current size.

In the process of accelerating the rotation of the turntable, the direction of the rotation axis of the wheel body changes rapidly, and the moment load borne by the supporting bearings at both ends increases continuously due to the conservation of angular momentum. The greater the angular acceleration, the faster the moment increases and the shorter the moment response time. According to the actual moment of inertia of the wheel body in the control moment gyroscope, when the speed increases from 0°/s to 60°/s during the acceleration of the turntable, the moment borne by the bearings at both ends of the wheel body increases from 0 N·m to 125 N·m. The friction torque of the bearing under different angular acceleration is measured respectively, and the results are as follows:

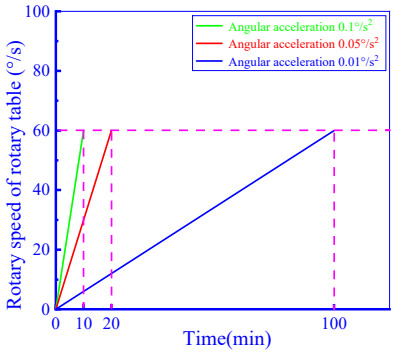

Figure 32. Rotary speed of rotary table.

Figure 33 shows that the friction torque of the bearing increases with the increase in the moment when the CMGB withstands a variable moment during the test. At the same time, when the torque load rises to a certain value (63 ± 5 N·m), the friction torque's fluctuation amplitude increases, similar to the simulation results. Moreover, the maximum error of friction torque between the test and the simulation result is 16.5%.

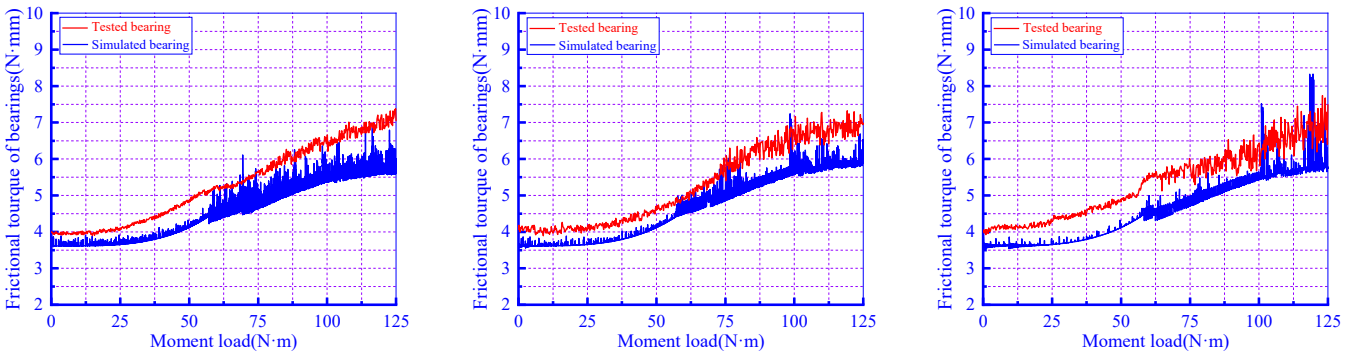

Figure 33. Friction torque fluctuation of bearing under the different angular accelerations.

4. Conclusions

(1) The friction torque fluctuation of CMGB is directly connected to the dynamic characteristics. When CMGB withstands a time-varying moment, the friction torque of the bearing increases with the increase in the moment, and the fluctuation of friction torque is related to the collision between the ball and the cage. For the different working conditions, there is a critical moment. If the moment is greater than the corresponding critical moment, the collision forces between the balls and cage increase; the axial displacement of the ball increases; the trajectory of the cage's mass center changes from irregular movement in a small range to the circular eddy motion; and the fluctuation of cage speed and friction torque will increase.

(2) When CMGB runs within the same moment range, the faster the time-varying moment response, the larger the collision forces between the balls and cage, the more irregular the trajectory of the cage's mass center, and the larger the fluctuation amplitude of the cage speed and friction torque.

(3) Under the condition of time-varying moment, the non-uniformity of the CMGB ball under load increases with the increase in torque load, and the raceway's binding force on the ball is insufficient after reaching the critical moment load, which increases the axial offset of the ball during the operation, and the amplitude of friction torque fluctuation increases. However, increasing the bearing preload can reduce the axial displacement of the ball and the fluctuation amplitude of the bearing friction torque within a certain range.

(4) Under the time-varying moments, with the increase in CMGB working temperature, the lubricant viscosity decreases, which increases the oil dumping rate of the porous oil

cage, reduces the friction coefficient between the contact surfaces of each part in the bearing, and reduces the fluctuation amplitude of the cage speed and friction torque.

Author Contributions: Conceptualization, W.Z.; methodology, N.Z.; validation, Y.Z.; writing—original draft preparation, S.L.; writing—review and editing, G.Z. and W.L. All authors have read and agreed to the published version of the manuscript.

Funding: This research received no external funding.

Data Availability Statement: Data are available upon request from the authors.

Conflicts of Interest: The authors declare no conflict of interest.

References

1. Zhang, Z.; Dong, W.; Zhang, J. The Application of Control Moment Gyro in Attitude Control of Tiangong-1 Spacecraft. *Aerosp. Control Appl.* **2011**, *37*, 52–59. [CrossRef]
2. Wei, D.; Li, G.; Fu, R.; Wu, D.; Zhang, J. Design of SGCMG and Long Life Rotor Bearing System Technology in Tiangong-1. *Sci. Sin. Technol.* **2014**, *44*, 261–268.
3. Lai, L.; Li, G.; Wu, D.; Zhai, B.; Ma, W. Miniature Control Moment Gyroscope for Small Satellites. *Aerosp. Control Appl.* **2017**, *43*, 43–48. [CrossRef]
4. Zhai, H.; Lai, L.; Wu, D.; Li, G.; Wei, W. Development and Application of Control Moment Gyroscope. *Aerosp. Control Appl.* **2020**, *46*, 1–7. [CrossRef]
5. Zhang, W.; Deng, S.; Chen, G.; Cui, Y. Impact of Lubricant Traction Coefficient on Cage'sdynamic Characteristics in High-speed Angular Contact Ball Bearing. *Chin. J. Aeronaut.* **2017**, *30*, 827–835. [CrossRef]
6. Popescu, A.; Houpert, L.; Olarua, D.N. Four Approaches for Calculating Power Losses in an Angular Contact Ball Bearing. *Mech. Mach. Theory* **2020**, *144*, 1–20. [CrossRef]
7. Gupta, P.K. Dynamic loads and cage wear in high-speed rolling bearings. *Wear* **1991**, *147*, 119–134. [CrossRef]
8. Han, Q.; Wen, B.; Wang, M.; Deng, S. Investigation of Cage Motions Affected by Its Unbalance in a Ball Bearing. *Proc. Inst. Mech. Eng. Part K J. Multi-Body Dyn.* **2018**, *232*, 169–185. [CrossRef]
9. Zhang, T.; Chen, X.; Gu, J.; Li, Q. Progress of Research on Cage Stability of High-Speed Angular Contact Ball Bearing. *Acta Aeronaut. Et Astronaut. Sin.* **2018**, *39*, 22026.
10. Wen, B.G.; Han, Q.K.; Qiao, L.C. Effacts of cage clearance on its wear in an angular contact ball bearing. *J. Vib. Shopck* **2018**, *37*, 9–14. [CrossRef]
11. Deng, S.; Li, X.; Wang, J.; Teng, H. Frictional Torque Characteristic of Angular Contact Ball Bearings. *J. Mech. Eng.* **2011**, *47*, 114–120. [CrossRef]
12. Wang, H.; Han, Q.; Luo, R. Dynamic modeling of moment wheel assemblies with nonlinear rolling bearing supports. *J. Sound Vib.* **2017**, *406*, 124–145. [CrossRef]
13. Wang, H.; Han, Q.; Zhou, D. Nonlinear dynamic modeling of rotor system supported by angular contact ball bearings. *Mech. Syst. Signal Process.* **2017**, *85*, 16–40. [CrossRef]
14. Dazhong, W.; Jiyang, Z.; Dengyun, W. Development of a 200Nms Single Gimbal Control Moment Gyro. *Aerosp. Control Appl.* **2011**, *37*, 14–18. [CrossRef]
15. Han, Q.; Jiang, Z.; Chu, F. Micro-vibration modeling and analysis of single-gimbal control moment gyros. *Commun. Nonlinear Sci. Numer. Simul.* **2023**, *118*, 107040. [CrossRef]
16. Zhang, D.; Wu, D.; Han, Q. Nonlinear dynamic force transmissibility of a flywheel rotor supported by angular contact ball bearings. *Nonlinear Dyn. Vol.* **2021**, *103*, 2273–2286. [CrossRef]
17. Longato, M.M.; Hughes, T.; Yotov, V. Microvibration simulation of reaction wheel ball bearings. *J. Sound Vib.* **2023**, *567*, 117909. [CrossRef]
18. Narayan, S.S.; Nair, P.S.; Ghosal, A. Dynamic interaction of rotating momentum wheels with spacecraft elements. *J. Sound Vib.* **2008**, *315*, 970–984. [CrossRef]
19. Sathyan, K.; Hsu, H.Y.; Lee, S.H.; Gopinath, K. A Bearing Cartridege Assembly for Long-Term Performance of Momentum/Reaction Wheels used in Spacecraft. *Tribol. Ind.* **2014**, *36*, 22–32.
20. Söchting, S.; Sherrington, I.; Lewis, S.D.; Roberts, E.W. An Evaluation of the Effect of Simulated Launch Vibration on the Friction Performance and Lubrication of Ball Bearings for Space Applications. *Wear* **2006**, *260*, 1190–1202. [CrossRef]
21. Hu, G.; Xu, Y.; Wu, J. Thermal Balance Test on a 200Nms Single-Gimbal CMG. *Aerosp. Control Appl.* **2008**, *34*, 25–28.
22. Taniwaki, S.; Kudo, M.; Sato, M.; Ohkami, Y. Analysis of Retainer induced Disturbances of Reaction Wheel. *J. Syst. Des. Dyn.* **2007**, *1*, 307–317. [CrossRef]
23. Wang, H.; Han, Q.; Zhou, D. Output Torque Modeling of Control Moment Gyros Considering Rolling Element Bearing induced Disturbances. *Mech. Syst. Signal Process.* **2019**, *115*, 188–212. [CrossRef]
24. Wang, Y.; Li, J.; Deng, S. Analysis on Temperature Field of Bearing Assembly for a Flywheel. *Bearing* **2015**, *10*, 24–28. [CrossRef]

25. Liao, H.; Xie, P.; Deng, S.; Zhang, W.; Shi, L.; Zhao, S. Investigation of Dynamic Characteristics Experiments and Stability Evaluation Criterion of Space Ball Bearing Cage. *Tribol. Trans.* **2023**, *66*, 453–465. [CrossRef]
26. Liao, H.; Xie, P.; Deng, S.; Zhang, W.; Shi, L.; Zhao, S.; Wang, H. Research on Early Fault Intelligent Diagnosis for Oil-impregnated Cage in Space Ball Bearing. *Expert Syst. Appl.* **2023**, *238*, 121952. [CrossRef]
27. Chen, S.; Chen, X.; Li, Q.; Gu, J. Experimental Study on Cage Dynamic Characteristics of Angular Contact Ball Bearing in Acceleration and Deceleration Process. *Tribol. Trans.* **2021**, *1*, 42–52. [CrossRef]
28. Ningning, Z.; Tao, Q.; Gang, Z. On the Friction Torque Properties of Bearing Assemblies in Fly Wheel. *Aerosp. Control Appl.* **2013**, *39*, 54–58.
29. Xia, X.; Chen, X.; Ye, L. Dynamic Prediction of Friction Torque Performance Reliability for Satellite Momentum Wheel Bearings. *China Mech. Eng.* **2013**, *30*, 1268–1275. [CrossRef]
30. Zhang, Y. The Influence of the Momentum Wheel Bearing Guide Surface Texture on the Dynamic Performance of the Cage. Master's Thesis, Harbin Institute of Technology, Harbin, China, 2019.
31. Wu, B.; Qing, T.; Zhou, N. Method to Estimate the Optimum Quantity of Lubricating Oil in Flywheel Bearing and Its Experimental Verification. *Aerosp. Control Appl.* **2014**, *40*, 42–47. [CrossRef]
32. Cui, Y.; Deng, S.; Deng, K.; Zhang, W.; Cui, Y. Friction Torque Characteristics of Control Moment Gyros Bearing Unit. *Aerosp. Control Appl.* **2020**, *46*, 73–80. [CrossRef]
33. Deng, K.; Xie, P.; Liao, H.; Zhou, G.; Deng, S. Mechanism of abnormal fluctuation of friction torque of control moment gyro bearing assembly. *J. Aerosp. Power* **2023**, *38*, 752–768. [CrossRef]
34. Deng, S.; Jia, Q.; Xue, J. *Rolling Bearing Design Principle*; Standards Press of China: Beijing, China, 2014.
35. Deng, S.; Hua, X.; Zhang, W. Analysis on Friction Torque Fluctuation of Angular Contact Ball Bearing in Gyro Motor. *J. Aerosp. Power* **2018**, *33*, 1713–1724. [CrossRef]